Top Catal (2013) 56:981–994
DOI 10.1007/s11244-013-0062-x

ORIGINAL PAPER

Effect of Metal-Support Interactions in Ni/ZSM-5 + Al_2O_3 Catalysts on the Transformation of *n*-Paraffins

A. Masalska · J. R. Grzechowiak · K. Jaroszewska

Published online: 17 May 2013

Abstract NiO(8 %)/Ni,H-ZSM-5 + Al_2O_3 (1:1) catalysts differing in metal-support interactions, which influenced the metal-to-acid ratios, were examined. The interactions were changed by modifying the method of zeolite and aluminium hydroxide combining and the method of Ni incorporation. The catalysts were characterised by ICP, XRD, N_2 sorption, SEM, TEM, NH_3-TPD, Py-IR, TPR, H_2 chemisorption and XPS. The effect of metal-support interactions was determined during *n*-C_6 conversion in a continuous system at H_2:CH = 7:1 Nm^3/m^3, 0.1 MPa and LHSV = 1 h^{-1}. It was found that over the catalysts with weaker Ni–alumina interactions (n_{Ni_a}/n, 3.2×10^{-2} and 4.8×10^{-2}), selectivity to isomerisation products was by 10–35 % higher, and selectivity to high boiling hydrocarbons by 10–30 % lower than over the catalysts with stronger Ni-support interactions (n_{Ni_a}/n, 1.2×10^{-2} and 1.8×10^{-2}).

Keywords Nickel catalyst · ZSM-5 + alumina · Metal-support interaction · *n*-Hexane

1 Introduction

Interactions between metal and oxide support affect such physicochemical properties of the catalyst as dispersion, size and metal crystallite distribution or acidity. The strength of the metal-support interactions depends largely on the type of metal and support, but is also influenced by the method of metal incorporation [1] and the type of active metal precursor [2–4].

Diverse methods of metal incorporation into the support have been reported in the literature. Among them, impregnation (dry or wet), ion exchange, co-precipitation, deposition via precipitation or vacuum vaporisation deserve particular attention [5–7]. When preparing catalysts with an active metal content higher than 10–20 wt%, preference is given to the precipitation method [5]. When catalysts of a lower active metal content are prepared, it is conventional to use the impregnation method. Since impregnation is concomitant with the adsorption of the metal precursor, knowledge of the pH value at which the support surface is neutral point of zero charge (PZC) becomes indispensable. When the pH of the solution is higher than the PZC of the support, the surface of the support is negatively charged and has therefore the ability to adsorb cations. With a pH value lower than that of PZC, the support surface has a positive charge and adsorbs anions [8–11].

Metal may be incorporated into the support/components of the support before or after the stage of support shaping [12]. When the support is a composite, the method of combining its components also gains in importance. When the active metal is incorporated prior to catalyst shaping, the components of the support (zeolite, alumina, silica) are predominantly powders of very fine grain size. Under such conditions, the interaction between the support and the metal precursor is a strong one, and the catalysts obtained via this route are in most instances characterised by a high metal content and good dispersion [13, 14]. Strong metal-support interactions contribute to the modification of metal and acid sites [15]. In some cases, however, strong interactions may produce an undesirable effect such as the formation of non-readily reducible compounds [16–19].

A. Masalska (✉) · J. R. Grzechowiak · K. Jaroszewska
Faculty of Chemistry, Wrocław University of Technology, Wrocław, Poland
e-mail: Aleksandra.Masalska@pwr.wroc.pl

In Ni/alumina systems, the interactions between nickel and alumina are influenced by the crystalline structure of alumina. The Ni/γ-Al_2O_3 system is characterised by the occurrence of strong metal-support interactions (SMSI), because nickel ions preferentially incorporate into the tetrahedral vacancies of γ-Al_2O_3 to form surface spinels ($NiAl_2O_4$). The Ni/θ–$A1_2O_3$ system displays weak metal-support interactions, because the amount of tetrahedral vacancies in θ-Al_2O_3 is low. Non-readily reducible spinels are catalytically inactive in hydrogenation reactions [20], thus limiting effective utilisation of the metal, although in some instances the presence of such spinels may be desired. Salagre et al. [21] observed that nickel aluminates had a stabilising effect on the reduced form of nickel (Ni^0). Barrio et al. [22, 23] arrived at a similar conclusion. The explanation for this phenomenon lies in the occurrence of electronic (Ni^0–Ni^{2+}) and geometrical effects attributable to the 'dilution' of Ni^0 by the non-reduced phase of Ni^{2+}. The study reported by Lif et al. [24] has disclosed that the stronger metal-support interaction between nickel particles and γ-Al_2O_3 suppresses diffusion of nickel particles and/or atoms and thus inhibits the sintering of the catalyst. Whilst investigating the Ni/γ-Al_2O_3 system in isoprene conversion, Wang et al. [25] found that when there was a sufficient number of hydrogenation sites on the catalyst surface, the presence of SMSI was able to resist carbon deposition. Sepulveda et al. [26] reported that a large proportion of Ni–Al oxide spinels enhanced the resistance of Ni catalysts to poisoning by sulphur compounds, and they attributed this effect to the trapping of H_2S by Ni^{2+}.

Transformation of *n*-paraffins (isomerisation/cracking) over bifunctional catalysts is described by two mechanisms: the monomolecular (classical) or the bimolecular one (dimerisation–cracking). The classical mechanism involves dehydrogenation of alkane to alkene on the metal sites. The alkene obtained adsorbs on the Brønsted acid site with the formation of the alkylcarbonium ion transition state followed by rearrangement, i.e. isomerisation [type *A*: via alkyl shift, type *B*: via protonated cyclopropane (PCP) intermediates, and eventually cracking (β-scission)]. At the final stage, on the metal site, the desorbed olefins undergo hydrogenation. The bimolecular mechanism (dimerisation–cracking) involves the reaction of alkene with the adsorbed tertiary carbenium ion (dimerisation) followed by its isomerisation and cracking (β-scission) [27]. The occurrence of the reactions governed by the monomolecular or bimolecular mechanism depends on the length of the alkene chain and the balance of the metallic and acidic function of the catalyst [28].

The selectivity of the catalysts towards the products of isomerisation or cracking is influenced by the average lifetime of the carbenium transition ions on the acid sites of the catalyst. A short lifetime promotes the isomerisation reaction and limits C–C bond cracking. The lifetime of carbenium ions can be shortened by reducing the proportion of strong acid sites, decreasing the pathway between metal sites and acid sites, and increasing the quantity of spill-over hydrogen, which facilitates alkene desorption. The character of the metal sites (type, amount, metal dispersion) and acid sites (type, density, acid strength) of the catalyst, as well as the ratio of the hydrogenating function to the acid function, have a decisive effect not only on the selectivity, but also on the activity of the catalyst. In the presence of catalysts with a low metal content, it is the metal function that acts as a factor limiting the reaction rate, because the number of metal atoms exerts a significant influence on the concentration of alkenes, and consequently on the activity of the catalyst. If the hydrogenating/dehydrogenating activity is sufficiently high to balance the acidity of the catalyst, the progress of the reaction is limited by the rearrangement of carbenium ions.

Activity and selectivity of the bifunctional catalyst depends on the character of its metal and acid functions, as well as on their balance, only if there are no diffusive limitations [29]. When the catalysts contain zeolites (or materials of zeolite type), their catalytic properties are influenced by the shape-selectivity phenomenon, whereas their activity and selectivity depend strongly on the geometry and dimensionality of the zeolite channel [30, 31].

This work attempts to ascertain how the catalyst preparation methods (zeolite combining/mixing with aluminium hydroxide, nickel incorporation) affect the metal-support interactions, and how these interactions influence the activity and selectivity of the catalysts in *n*-hexane transformation.

2 Experimental

2.1 Catalyst Preparation

Ni catalysts (8 wt % NiO) supported on Al_2O_3 + Ni,H-ZSM-5 (1:1) (Table 1) were prepared. The preparation of series A catalysts involved aging of a mixture of zeolite and aluminium hydroxide powders in water, followed by their peptisation (1 % HNO_3). The preparation of series E catalysts entailed a mixture of two pastes obtained separately: zeolite (with 1 % HNO_3) and peptisate of aluminium hydroxide (with 1 % HNO_3). Nickel [nickel(II) nitrate(V)] was added before the stage of support shaping (method F), by impregnation of the support already formed and calcined (method I) or by a two-stage method (F + I), where half of the metal was incorporated before support shaping, and the other half was added by impregnation. When the active component was incorporated before catalyst shaping and use was made of method E (combination of zeolite and aluminium hydroxide pastes), $Ni(NO_3)_2$ was

Table 1 Preparation method and texture of nickel catalysts

Code	Preparation method		Specific surface area (m^2/g)		Pore volume (cm^3/g)			Pore diameter (nm)	
	ZSM-5 and Al_2O_3 combining	NiO deposition	S_{BET}	S_t^a	V_T^b	V_{MES}	V_{MIC}^a	APD[c]	d_{BJH}^d
A/F + I	A	F + I	269	233	0.35	0.29	0.039	5.2	5.6
A/F	A	F	298	234	0.36	0.33	0.028	5.0	4.9
E/I	E	I	283	231	0.35	0.31	0.029	5.0	5.6
E/F + I	E	F + I	258	192	0.35	0.30	0.032	5.5	5.6
E/F	E	F	269	176	0.33	0.27	0.041	4.9	5.1

Methods of zeolite and alumina combining: A—powders of aluminium hydroxide and zeolite are mixed in an aqueous solution, E—two pastes prepared separately are combined: Ni,H-ZSM-5 zeolite with 1 % HNO_3 and aluminium hydroxide peptisate (obtained with 1 % HNO_3). Methods of Ni incorporation: F—before shaping, I—by impregnation of shaped support

[a] *t*-plot method

[b] At $p/p_0 = 0.99$

[c] Average pore diameter

[d] Pore diameter determined from desorption branch by the BJH method

added during peptisation of aluminium hydroxide (to prevent metal deposition on the active sites of the zeolite and/or blocking of the zeolite's channels). In series A catalysts, nickel precursor was added to a zeolite and aluminium hydroxide mixture. Extrudates were dried at 110 °C for 18 h and then calcined at 480 °C for 3 h.

2.2 Catalyst Characterisation

The catalysts were characterised by N_2 sorption (at 77 K), TPR (up to 850 °C), ICP, XRD, SEM, TEM, H_2 chemisorption, XPS, NH_3-TPD and Py-IR. When use was made of H_2 chemisorption and XPS, the catalysts were reduced in H_2 at 500 °C.

2.2.1 Porous Structure and Acidity

N_2 adsorption was measured at 77 K making use of a Quantachrome Autosorb Automated Gas Sorption System. Before each measurement, the sample was outgassed under vacuum conditions at 150 °C for 1 h. Acidity was determined by temperature-programmed desorption of ammonia (NH_3-TPD) and by adsorption of pyridine (Py-IR). In the ammonia method, acidity and acid strength distribution were evaluated in a through-flow system using a katharometer as a detector. More details can be found in a previous paper [32]. Prior to acidity measurement by pyridine (Py) chemisorption, the samples were activated at 530 °C for 1 h. Adsorption was carried out at 170 °C, and the excess of pyridine was placed in the cell. IR spectra were recorded at room temperature making use of a BRUKER 48 PC spectrometer equipped with an MCT detector. Acid site concentrations were measured using the Py absorption bands of 1,450 and 1,545 cm^{-1} for Lewis (PyL) sites and Brønsted (PyH^+) sites, respectively.

2.2.2 Chemical Analysis and H_2 Chemisorption

Ni was determined with an inductively coupled plasma-atomic emission spectrometer (ICP-AES PU 7000 from Philips, Cambridge UK) connected with an ultrasonic nebuliser CETAC (USA). H_2 volume adsorbed was measured with a Micromeritics ASAP 2010C instrument. Samples were reduced in a H_2 stream at 500 °C (1 h).

2.2.3 TPR Experiments

The TPR of the catalyst was conducted to the temperature of 850 °C, using a mixture composed of 80 vol% of Ar and 20 vol% of H_2 (>99.999 %); gas velocity and heating rate were 40 cm^3/min and 15 °C/min, respectively. Before each TPR run, the samples were oxidised in an argon stream containing 15 vol% of O_2 at 500 °C for 30 min. Tests were performed using an Altamira AMI-1 system.

2.2.4 XRD Measurements

XRD patterns were obtained with a PANalytical X'Pert ProMPD diffractometer coupled to a PW3050/65 high resolution goniometer, at 40 kV and 30 mA (CuKα). Data were collected over the 2θ range of 5–90° with a step size of 0.0167 and a 25.8-second time per step. These diffractograms were compared with a diffractogram taken from the JCPDX index.

2.2.5 X-ray Photoelectron Spectroscopy

XPS examinations were carried out making use of a SPECS PHOIBOS 100 spectrometer with Mg Kα radiation. The spectrometer was calibrated with the Au $4f_{7/2}$, Ag $3d_{5/2}$ and Cu $2p_{3/2}$ lines at 84.2, 367.9 and 932.4 eV,

respectively. The Al 2p line (at 73.83 eV) was used as a reference. A nonlinear least-square fitting algorithm was applied using peaks with a mix of Gaussian and Lorentzian shape and a Shirley baseline.

2.2.6 Surface Morphology

SEM was performed using a JSM5800LV microscope (JEOL) with an ISIS300 system for microanalysis (Oxford). Micrographs were obtained at 20 kV. HRTEM images and selected area electron diffraction (SAED) patterns were obtained with a Philips CM-20 SuperTwin microscope.

2.3 Catalytic Activity Tests

Catalytic activity was tested in the transformation of *n*-hexane (*n*-C_6) for two reasons. Firstly, the kinetic diameter of this hydrocarbon enables penetration of the ZSM-5 channels without steric hindrance. Secondly, *n*-hexane contains such a number of carbon atoms that permits not only its isomerisation and cracking, but also dehydrocyclisation and aromatisation. Activity measurements were carried out in a continuous-flow system (fixed-bed reactor, 8.0 mm i.d.) with *n*-C_6 saturated hydrogen flow (>99.8 %). Before each determination procedure, the samples (3 cm^3, 0.50–0.75 mm) were activated with hydrogen (450 °C, 3 h). Experiments were conducted at H_2:CH = 7:1 Nm^3/m^3 and LHSV = 1 h^{-1}. Reaction products were analysed by the GC method (N-504, FID) using the RTX-1 capillary column (100 % dimethylpolysiloxane, 60 m/0.25 μm). Results are reported as conversions (percent of *n*-C_6 reacted) and selectivities to reaction products (weight percent of reaction product to conversion).

3 Results and Discussion

3.1 Morphology, Texture and Acidity

The XRD diffractograms obtained did not very much differ from one another. They displayed a signal characteristic of Ni,H-ZSM-5 (signal split at 2θ of 23.10°) and broad signals from γ-Al_2O_3. None of the catalysts tested had X-ray diffraction lines characteristic of stoichiometric compounds such as NiO and $NiAl_2O_4$, and none of them displayed signals at 2θ of 32.2, 37.4, 45.5, 57.5, 60.6, and 66.5°, which (according to JCPDS: 20–776, 20–777, 37–1292, 10–339) could be associated with non-stoichiometric Ni–Al oxide spinels of the general formulation $Ni_xAl_{(8/3-2/3x)}O_4$ (where $0 < x < 1$). A typical diffractogram of the A/F + I catalyst is shown in Fig. 1.

Surface morphology determined by SEM has revealed that catalysts of series A and series E noticeably differ in the extent of zeolite and alumina separation. Figures 2 and 3 show SEM images of A/F + I and E/F + I catalysts (with indicated regions of microanalysis) and X-ray spectra of the regions chosen.

Analysis of the spectra (20 kV) in Fig. 2b, c, e and those in Fig. 3b, c makes it clear that the Al_2O_3 layers covering the Ni,H-ZSM-5 crystals are thicker in A/F + I than in E/F + I. That the zeolite is covered with Al_2O_3 layers can be seen from the measured results obtained at the same points with accelerating voltage of 20 and 15 kV, respectively. The ratio of the countings of Si atom numbers to the countings of Al atom numbers for the spectra obtained at 15 kV is lower than the same ratio for the spectra obtained at 20 kV (Fig. 2, comparison of spectra c–d, e–f and h–i). This difference should be attributed to the lower depth from which X-rays were emitted.

SEM micrographs of catalyst surfaces have confirmed that the combination of zeolite and aluminium hydroxide by method A yields a better blend of the components than does their combination by method E (Fig. 4). In E/F + I and E/F, silica is located in the voids of the Al micrographs. This location is less distinct in the A/F + I micrograph.

SEM micrographs of Ni distribution show that nickel did not migrate from alumina to zeolite crystals during preparation involving intense mixing of pastes and calcination. The coverage of E/F + I zeolite crystals with nickel is good, because during catalyst preparation only half of the metal was incorporated at the stage when zeolite and aluminium hydroxide pastes were combined, the other half being added by impregnation. It is worth noting that when use is made of a nickel(II) nitrate(V) solution with a pH of 4.8, it can be expected that adsorption onto the zeolite crystal (PZC of about 4) will be better than onto alumina grains (PZC of about 7–8) [10]. The most uniform Ni distribution was observed on the surface of A/F + I.

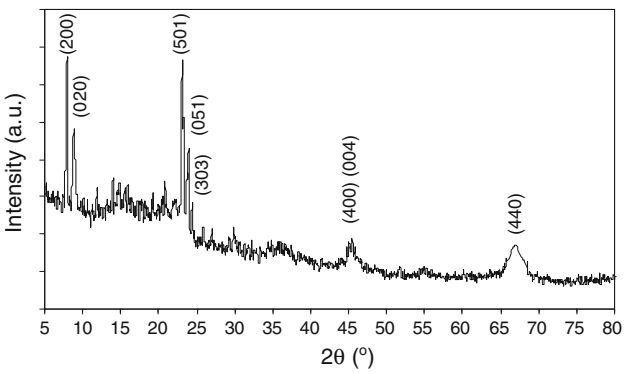

Fig. 1 XRD pattern of 8 %NiO/Ni,H-ZSM-5 + Al_2O_3 catalyst (A/F + I)

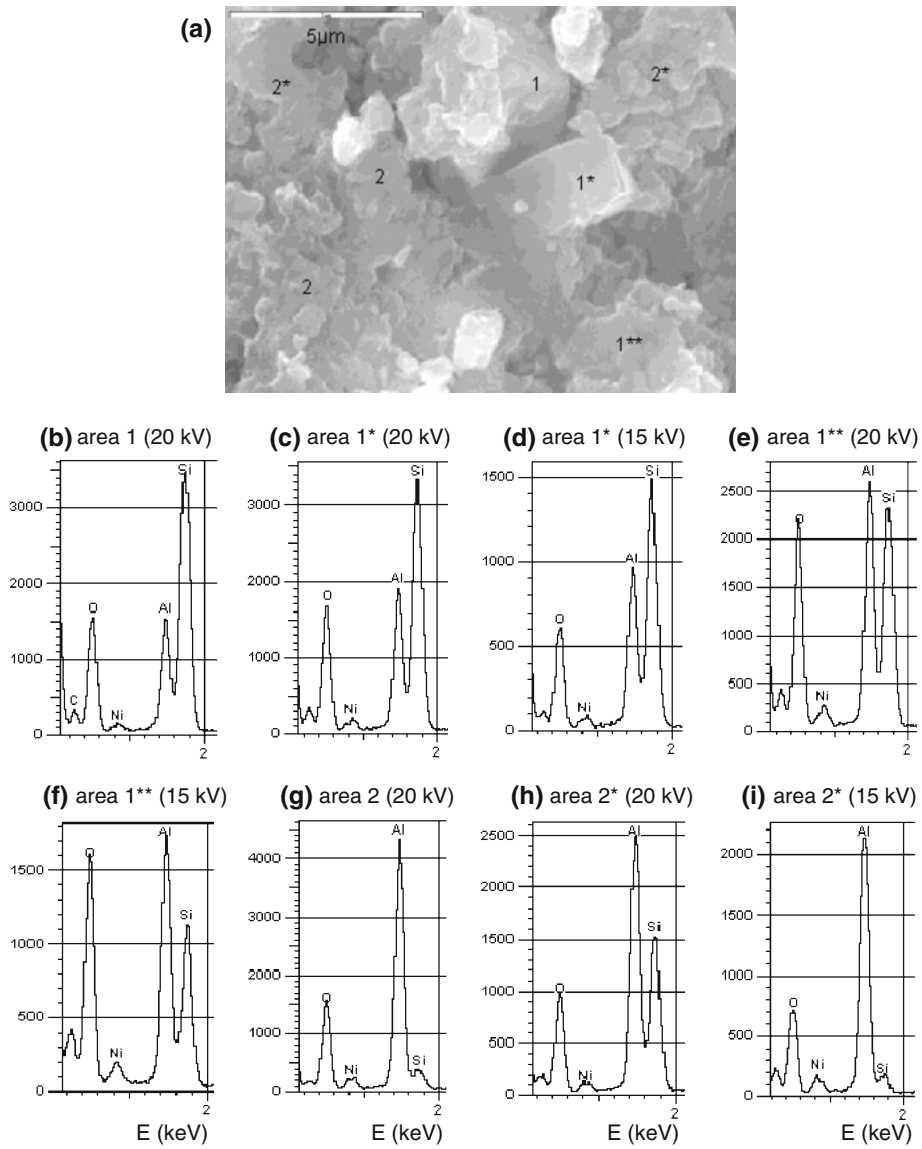

Fig. 2 SEM micrograph of A/F + I catalyst with marked areas of analysis (**a**), and X-ray spectra (**b–i**)

The preparation method had an influence on Ni distribution not only on the catalyst surface, but also along the extrudate's cross-section. Local Ni concentrations (determined every 150 μm with an X-ray probe) are presented in Fig. 5. The smallest differences are observed for E/F when during preparation the whole Ni amount was incorporated before catalyst shaping. Ni incorporation by the two-stage method (A/F + I, E/F + I) accounted for the increase in the Ni amount on the external surface of the extrudate as well as for the simultaneous reduction in the Ni content of the successive layers. The greater is the reduction, the smaller is the average pore diameter (A/F + I) (Table 1).

In this work, the TEM patterns of the A/F + I and E/F catalysts were taken as examples (Figs. 6, 7). The electron diffraction patterns of the two catalysts display rings typical of γ-Al_2O_3 (at 2.37, 1.97 and 1.39 Å) as well as reflections characteristic of nickel (at 2.03, 1.76, 1.24 and 1.05 Å) (Figs. 6a, 7a).

The microstructure of alumina grains in the A/F + I catalyst (where half of the Ni amount was incorporated into the mixture of aluminium hydroxide and zeolite before shaping, and the other half into 4 % NiO/zeolite + Al_2O_3 by impregnation) has revealed the presence of nickel crystallites, which range in size from 7 to 19 nm (Fig. 6a–d). In the E/F catalyst (where the whole Ni amount was incorporated into aluminium hydroxide), nickel crystallites of alumina grains show differences in size. Among these crystallites, those varying between 5.5 and 8 nm are dominant (Fig. 7a, b), but there are also larger crystallites, whose size ranges from 20 to 35 nm (Fig. 7c, d), with distinct 0.20 nm spectral lines associated with Ni (111). The difference in Ni distribution on the zeolite crystals

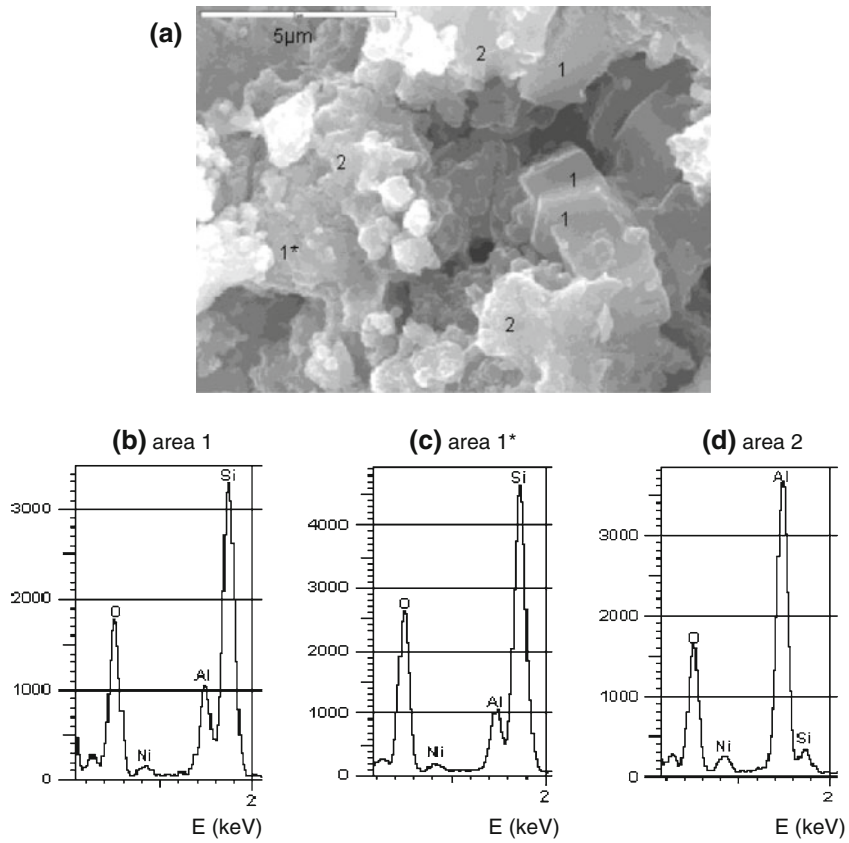

Fig. 3 SEM micrograph of E/F + I catalyst with marked areas of analysis (**a**), and X-ray spectra (20 kV) (**b–d**)

between the two catalysts (Fig. 6e, f and Fig. 7e, f) is attributable to the method used for Ni incorporation. In the E/F catalyst, the zeolite crystals in some instances exhibit small Ni crystallites, whereas in the A/F + I catalyst they display large ones (13–28 nm).

The catalysts have an S_{BET} of 258–298 m^2/g, a pore volume of 0.33–0.36 cm^3/g and an average pore diameter of 4.9–5.5 nm (Table 1). The lowest micropore volume was detected in the E/I catalyst, where the whole Ni amount was incorporated by impregnation after support shaping, and also in the A/F catalyst, where the whole Ni amount was added to the mixture of zeolite and aluminium hydroxide powders (0.029 and 0.028 cm^3/g, respectively). The micropore volume of the other catalysts ranges between 0.032 and 0.041 cm^3/g.

Py-IR measurements show that in all of the catalysts Lewis acid sites are dominant, and that the PyH^+/PyL ratios vary from 0.25 to 0.29 (Table 2). E/F and A/F + I catalysts are characterised by the highest PyH^+ acidity. Total acidity determined by the NH_3-TPD method falls in the range of 0.82 mmol NH_3/g (A/F + I) to 0.89 mmol NH_3/g (E/F). From the acid strength distribution it follows that in every instance about 50 % of acidity is associated with such sites where ammonia is desorbed over the temperature range of 300–450 °C(M). The proportion of the sites defined as S^+, namely those releasing ammonia at temperatures higher than 550 °C, is the highest with E/I and A/F catalysts.

3.2 Characteristics of Metal Function and Metal-Support Interactions

To characterise the metal function of nickel catalysts and the Ni-support interactions, measurements were performed to determine their reducibility (TPR), H_2 chemisorption (metal surface, S_M; volume of H_2 adsorbed, V_{H2}; dispersion, D) and chemical composition of the catalyst surface (XPS). The ICP measurement shows that the Ni amount is close to the assumed one and ranges from 7.9 to 8.3 wt% of NiO.

In the Ni/zeolite + alumina catalysts, interaction between nickel and zeolite is poor compared with the interaction between nickel and alumina. In the case of hydrothermal or acid treatment (which leads to dealumination), Ni–Al spinels may form as a result of Ni^{2+} reaction with EFAL [33, 34]. In this work, the Ni-support interactions are considered as interactions between nickel and aluminium hydroxide/alumina.

TPR profiles of the catalysts (except that of E/I) display main reduction areas with maxima at between 780 and 800 °C as well as small reduction areas with maxima at about 450 °C (Fig. 8). For E/I, the main reduction area

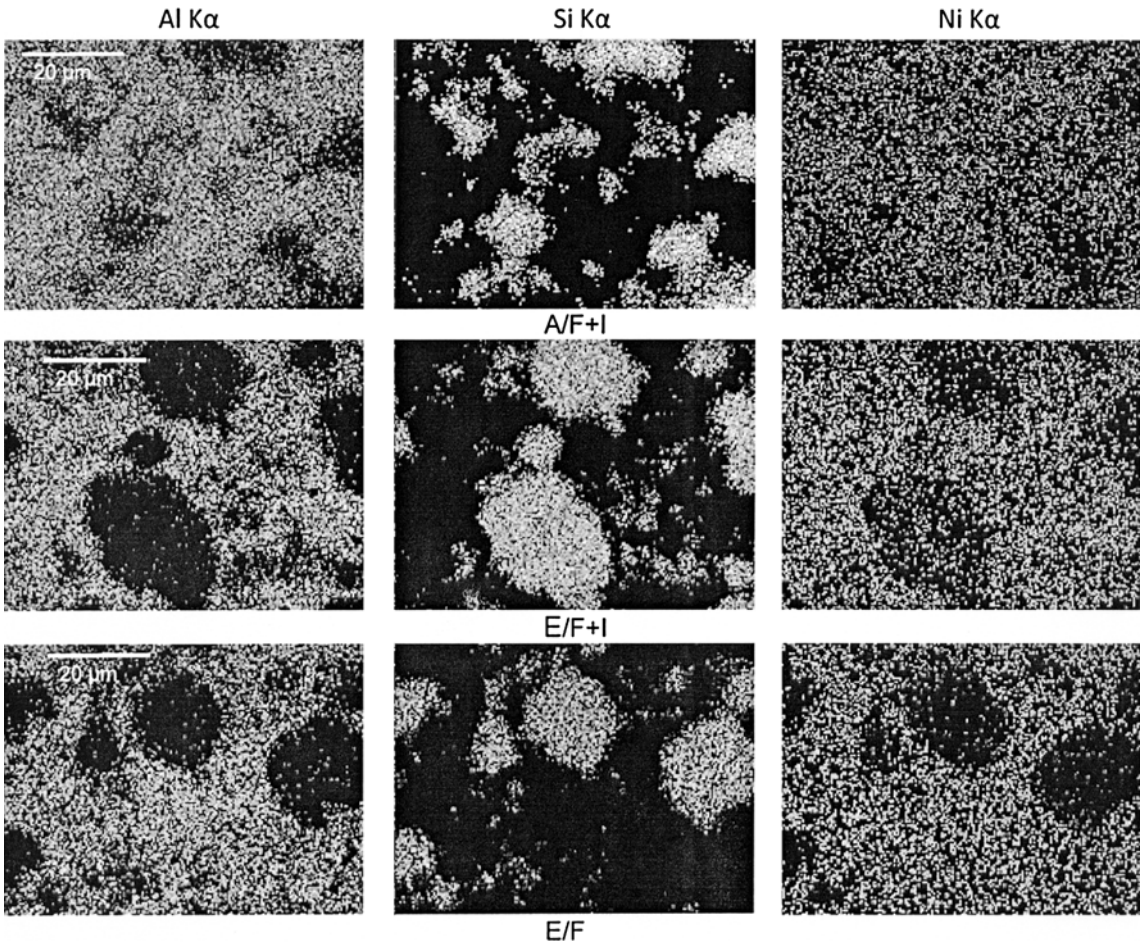

Fig. 4 SEM micrographs of the catalysts: distribution of aluminium, silica and nickel on catalyst surfaces

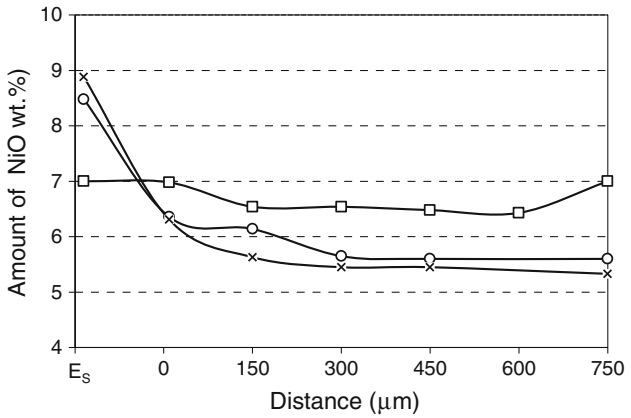

Fig. 5 Nickel distribution along the cross-section of the extrudates. External surface (E_S), internal edge of the extrudates (0 µm), centre of the extrudates (750 µm). Catalysts: A/F + I (*times*), E/F + I (*white circle*), E/F (*white square*)

falls within the range of 550–800 °C. The occurrence of nickel oxides, which strongly differ in reducibility, is associated with the presence of Ni–Al spinels and amorphous nickel oxide layers, which are not chemically bound but interact (more or less strongly) with alumina [35]. Reduction in spinel structures occurs at temperatures higher than 700 °C, whereas reduction in amorphous nickel oxide layers is observed within the range of 380–690 °C. Analysis of TPR profiles in this study has revealed that a strong interaction between nickel(II) nitrate(V) and aluminium hydroxide occurred during the preparation procedure, which produced non-readily reducible spinel structures. A strong interaction between NiO and aluminium hydroxide/alumina, which had led to the formation of Ni–Al spinels, was also reported by other investigators [16, 36–38].

As can be seen from the data in Table 3, all the catalysts tested are characterised by low nickel dispersion (0.9–3.7 %). Nickel dispersion and hydrogen uptake to the temperature of 500 °C (calculated based on TPR measurements) in catalysts where the entire nickel amount (E/I) or half of the nickel amount (A/F + I, E/F + I) was incorporated by impregnation are slightly higher than in catalysts obtained by metal precursor incorporation prior to shaping (A/F, E/F) (Table 3). The explanation for the low Ni dispersion in the catalysts examined (determined upon

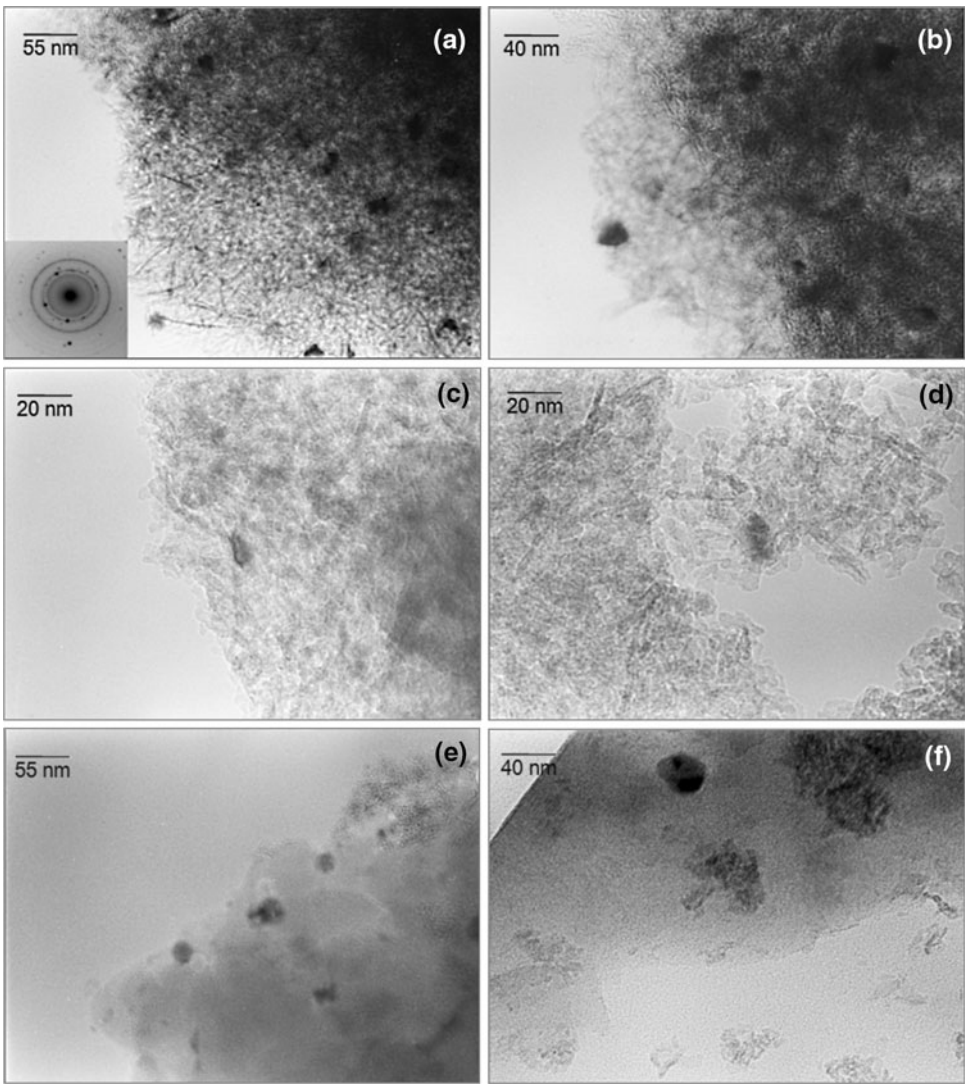

Fig. 6 TEM micrographs of A/F + I catalyst: alumina grains (**a**–**d**) and zeolite crystals (**e**, **f**)

reduction at 500 °C) lies in the poor reducibility of nickel oxides confirmed by TPR measurement.

To determine the chemical composition of the catalyst surface, use was made of the XPS technique (Table 4). Relative Ni atom concentration (Ni/Al + Si atomic ratio) on the surfaces of A/F + I, E/F + I and E/I catalysts is slightly higher than on the surfaces of the catalysts prepared via incorporation of the whole assumed Ni amount by method F (A/F, E/F). The data in Table 4 also characterise the proportions of nickel corresponding to its energy states associated with nickel occurrence in different chemical compounds.

Based on the deconvolution of the Ni $2p_{3/2}$ spectra obtained for A/F + I after reduction at 800 °C (Fig. 9a) and calcination at 1,100 °C (Fig. 9b), the following binding energies have been assumed (B_E): 852.8 eV for Ni^0, 855.3 eV for NiO, and 857.9 eV for $NiAlO_4$. These values are similar to those reported in the literature for metallic Ni^0 (853.0 eV [21]), NiO (854.0–855.0 eV [21, 39]) and $NiAlO_4$ (856.5–857.8 eV [21, 33, 39, 40]).

XPS results substantiate the low reducibility of nickel catalysts at 500 °C (detected in TPR). Ni^0 content (at%) on catalyst surface did not exceed 20 % (Table 4). Regardless of the method used for combining zeolite with aluminium hydroxide, Ni^0 content was higher on the surfaces of such catalysts where nickel was incorporated by method I or F + I (11–18 %) than on the surfaces of the catalysts obtained by method F (7–9 %). The strong interaction between nickel and aluminium hydroxide/alumina (that occurs during impregnation and calcination) is confirmed by the high amount of Ni–Al spinels.

In sum, metal-support interactions are strong in all the catalysts tested. This finding has been substantiated by TPR, H_2 chemisorption and XPS. But detailed analysis shows that when the whole quantity of nickel precursor is incorporated before catalyst shaping (A/F, E/F), metal-support interactions are slightly stronger than when nickel precursor is deposited by single-stage impregnation (E/I) or

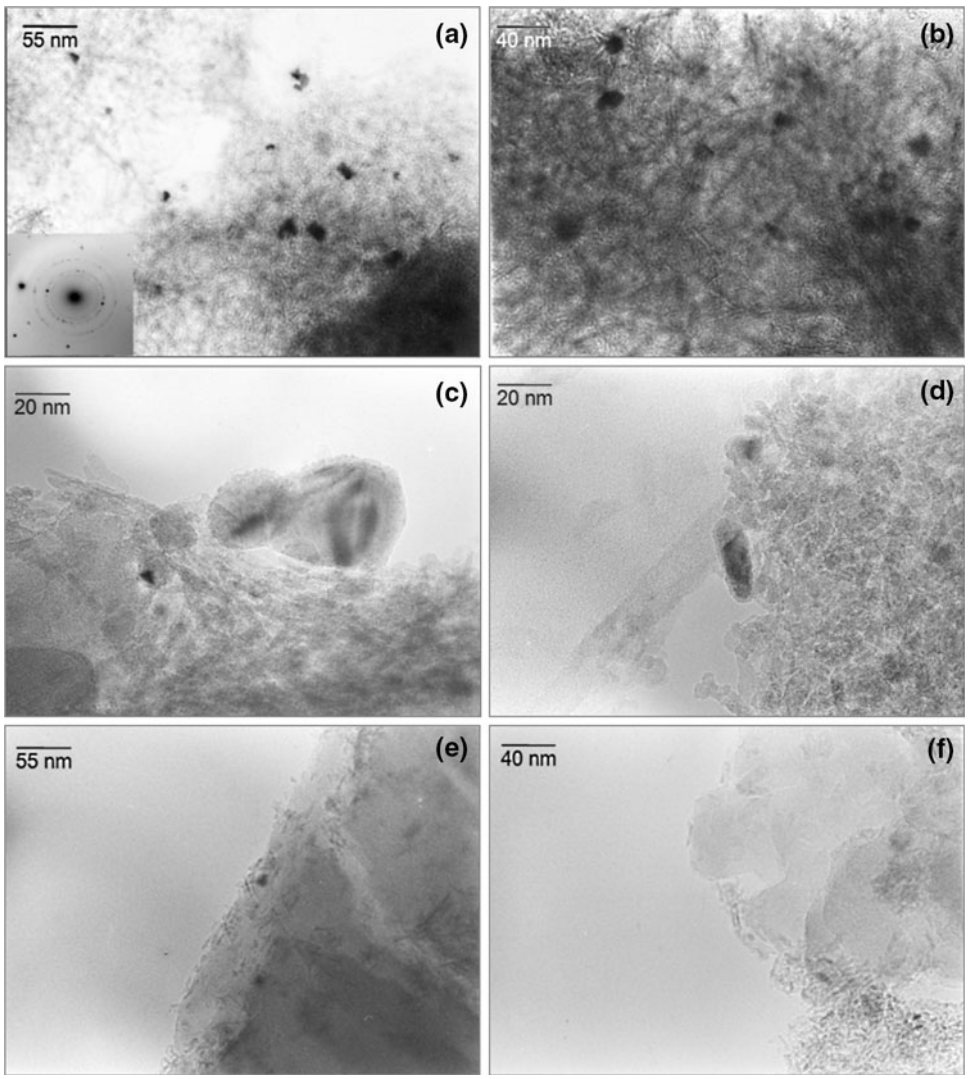

Fig. 7 TEM micrographs of E/F catalyst: alumina grains (**a**–**d**) and zeolite crystals (**e**, **f**)

Table 2 Acidity of nickel catalysts

Code	NH_3-TPD (mmol/g)					Py-IR (mmol/g)		
	W	M	S	S^+	Σ	PyH^+	PyL	Σ
A/F + I	0.11	0.46	0.24	72	0.82	0.17	0.62	0.72
A/F	0.14	0.46	0.23	97	0.83	–	–	–
E/I	0.13	0.49	0.26	95	0.88	–	–	–
E/F + I	0.16	0.46	0.24	78	0.86	0.14	0.55	0.69
E/F	0.15	0.50	0.24	73	0.89	0.18	0.63	0.80

W, M, S—acid sites desorbed NH_3 at 180–300, 300–450 and 450–550 °C, respectively, S^+—intensity of the signal at 550 °C (mm), PyH^+—Brønsted acid sites, PyL—Lewis acid sites

by the two-stage method involving impregnation at the second stage (A/F + I, E/F + I).

The acidities of these catalysts are comparable, so it was possible to characterise the metal-support interactions by the ratio of the number of accessible Ni^0 atoms (n_{Ni_a}) to the total number of acid sites determined by NH_3-TPD (n). However, this ratio, which is of significance to bifunctional catalysts, does not include the slight differences either in the distribution or in the strength of acid sites. Catalysts prepared by impregnation with the single-stage method (E/I) or by the two-stage method where one-half of the metal was incorporated by impregnation (A/F + I, E/F + I) display higher metal-to-acid ratios (n_{Ni_a}/n, 2.7–4.8 × 10^{-2}) than do the catalysts prepared by method F of metal incorporation (A/F, E/F) (n_{Ni_a}/n, 1.2 and 1.8 × 10^{-2}).

3.3 Catalytic Activity: Transformation of *n*-Hexane

The activity and selectivity of the catalysts in n-C_6 transformation, as well as the distribution of the reaction products, are shown in Figs. 10 and 11 and summarised in Tables 5 and 6. The reaction products have been divided into the following groups: (i) C_{1+2} hydrocarbons, (ii) C_3–C_5 hydrocarbons (both produced in the cracking reaction), (iii) i-C_6 isomerisation products, and (iv) hydrocarbons

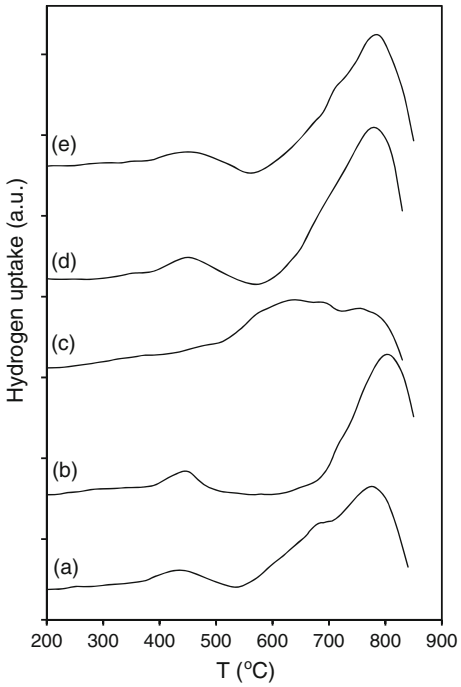

Fig. 8 Effect of the preparation method on the reducibility of nickel catalysts. TPR profiles of catalysts: A/F + I (**a**), A/F (**b**), E/I (**c**), E/F + I (**d**), E/F (**e**)

Table 3 Characteristics of metal function (8 %NiO/Ni,H-ZSM-5 + Al_2O_3)

Code	V^a_{H2} (cm^3/g)	S^b_M (m^2/gNi)	D^c (%)	H_2 uptake up to 500°C[d] (cm^3/g)	$n_{Nia}/n \times 10^2$
A/F + I	0.404	22.3	3.7	7.3	4.8
A/F	0.103	5.70	0.9	3.2	1.2
E/I	0.267	14.81	2.2	7.8	2.7
E/F + I	0.310	17.09	2.6	5.8	3.2
E/F	0.181	10.03	1.5	5.2	1.8

[a] Volume of H_2 chemisorbed

[b] Metallic surface

[c] Dispersion

[d] H_2 uptake up to 500 °C (TPR), n_{Ni_a} = amount of accessible nickel atoms, n = amount of total acid sites (NH_3-TPD)

with boiling points higher than those of n-C_6 (HBH). Since the formation of the cracking products is governed by different reaction mechanisms, they have been classified into C_{1+2} and C_3–C_5 groups. Methane and ethane (C_{1+2}) are very likely to be produced via cracking on metals (hydrogenolysis), because their production over metal/acid catalysts cannot be explained by the classical monomolecular bifunctional mechanism, which would imply the formation of very unstable primary carbenium ions. It should be noted, however, that C_{1+2} (as well as H_2) may form over a monofunctional acid catalyst or bifunctional catalyst with a poor hydrogenating function, when alkane conversion occurs according to the monomolecular reaction mechanism via a non-classical, penta-coordinated carbonium ion. In contrast to other mechanisms of alkane conversion over a monofunctional acid catalyst (such as the bimolecular mechanism including H-transfer and occurring via a tri-coordinated carbenium ion; or the oligomeric mechanism involving alkylation reactions), the monomolecular non-classical mechanism is preferred when conversion is low and reaction temperature is high.

The results of the tests obtained with catalysts of series A and E in n-C_6 transformation demonstrate that at reaction temperatures higher than 300 °C the conversions of n-C_6 over the catalysts tested (except A/F at 400 °C) are similar (Table 5).

Hydrocarbon conversion on metallic sites always competes with hydrocarbon conversion via the bifunctional mechanism. The contribution of metallic sites gains in importance under severe reaction conditions and also in the environment of weak zeolite acidity. The selectivities of the catalysts toward hydrogenolysis and cracking products are shown in Fig. 10a, b. As can be seen from Fig. 10a, selectivity to C_{1+2} is higher over A/F + I and E/F + I than over the other catalysts. Weaker Ni–alumina interactions in these catalysts account for the greater amount of metal sites on their surfaces; these metal sites are active in hydrogenolysis.

The maximum on the plot of C_3–C_5 selectivity (Fig. 10b) observed in all the catalysts examined suggests that C_3–C_5 hydrocarbons undergo secondary cracking/

Table 4 XPS characteristics of catalyst surface (after reduction at 500 °C, 1 h)

Code	Surface atomic chemical composition (%at)				Atomic ratio Ni/Al + Si	Relative amount of Ni (%at)		
	O	Al	Si	Ni		Ni^o/Ni_{total} (852.8 eV)	NiO/Ni_{total} (855.3 eV)	$NiAlO_4/Ni_{total}$ (857.9 eV)
A/F + I	63.0	32.6	3.1	1.31	0.037	14	40	46
A/F	62.4	34.6	2.1	0.87	0.024	9	40	51
E/I	65.1	30.2	3.3	1.38	0.041	18	41	41
E/F + I	62.6	31.5	4.6	1.27	0.035	11	46	43
E/F	62.5	34.3	2.0	1.21	0.033	7	41	52

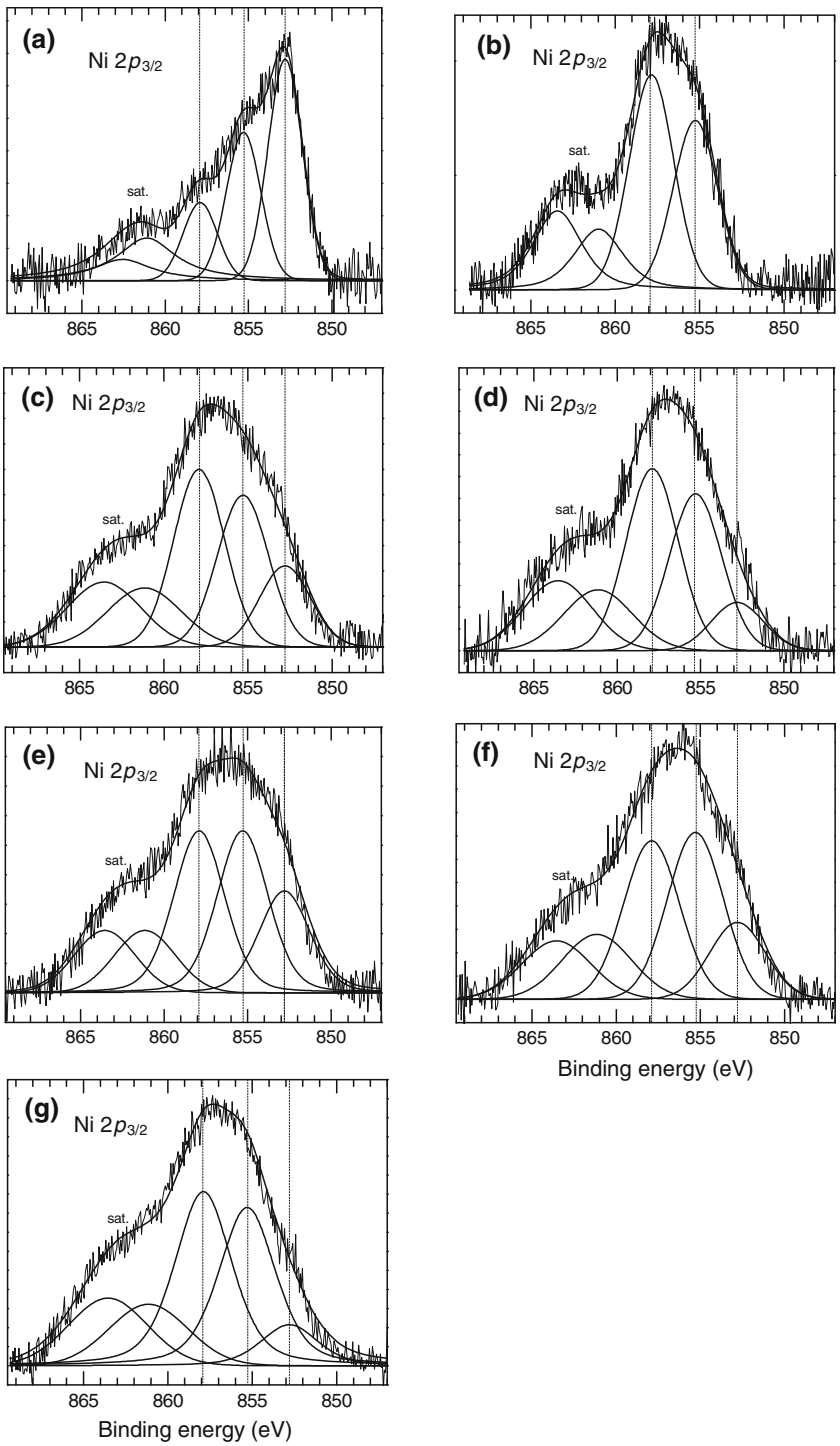

Fig. 9 XPS spectra of Ni $2p_{3/2}$ region for catalysts: A/F + I after reduction at 800 °C (**a**), A/F + I after calcination at 1,100 °C (**b**), as well as for catalysts: A/F + I (**c**), A/F (**d**), E/I (**e**), E/F + I (**f**), E/F (**g**), all after reduction at 500 °C

hydrogenolysis and/or play an important role in HBH formation (polymerisation/alkylation and aromatisation).

The distribution of cracking products is shown in Fig. 11 (as the percentage of C_1 to C_5 hydrocarbons in the C_1–C_5 cut). Cracking products are also characterised by the following parameters: the h/c ratio (the number of n-$C_{6\ mol}$ converted to C_{1+2} to the number of n-$C_{6\ mol}$ converted to C_3–C_5 hydrocarbons), the fragmentation factor, ζ, and the *i/n* ratio for the $C_4 + C_5$ fraction (Table 6). The ζ value represents the number of moles of hydrocarbon fragments per mole of n-C_6 cracked ($\zeta = \Sigma C_i/\Sigma iC_i/6$).

Product distribution within the C_1–C_5 fractions (taken as an example at conversion of about 60 %) indicates that propane is not the only cracking product (Fig. 11). But propane would be the only product if *n*-hexane cracking occurred according to the classical bifunctional

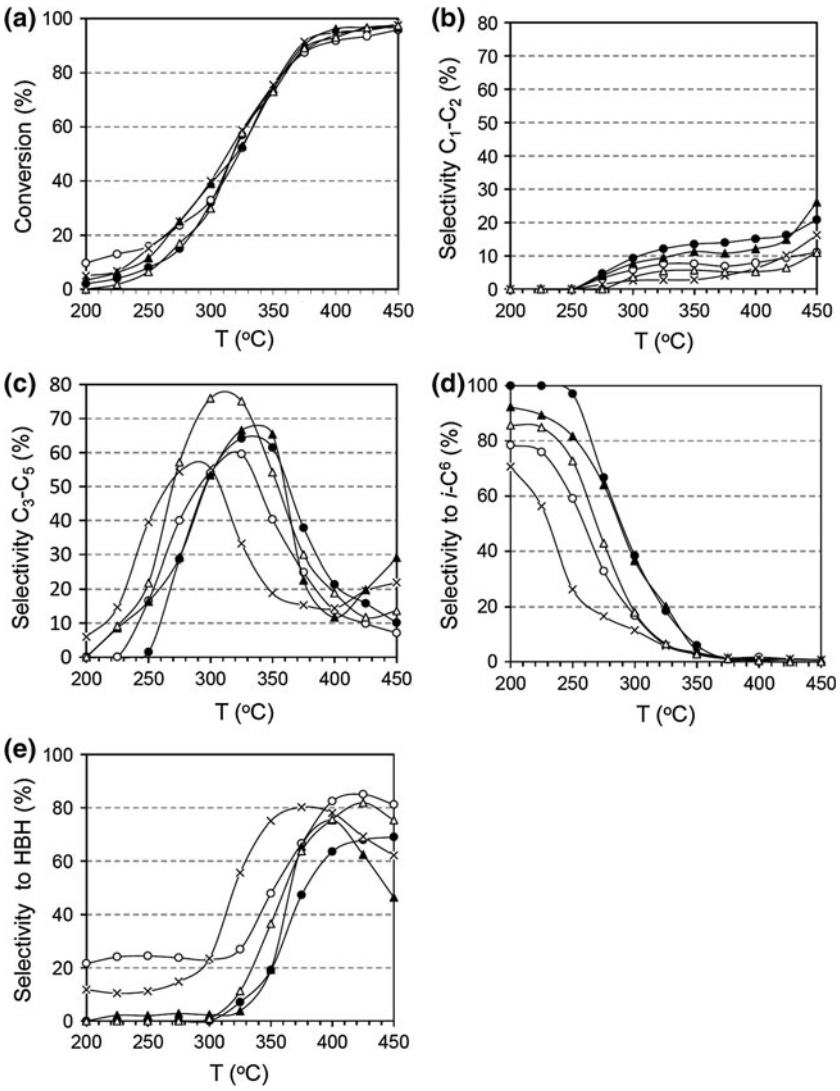

Fig. 10 Effect of preparation method on the activity of 8 wt% NiO catalysts. Conversion of *n*-hexane (**a**), selectivity to hydrocarbons: C_{1+2} (**b**), C_3–C_5 (**c**), *i*-C_6 (**d**) and HBH (**e**). Catalysts: A/F + I (*filled circle*), A/F (*white circle*), E/I (*times*), E/F + I (*filled triangle*), E/F (*white triangle*)

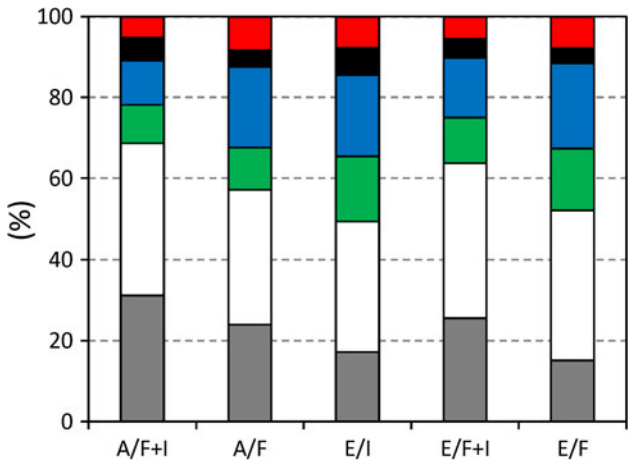

Fig. 11 Distribution within C_1–C_5 fraction: C_{1+2}, C_3, iC_4, nC_4, iC_5, nC_5

monomolecular mechanism, because β-scission of the carbenium ion that contains six carbon atoms occurs solely according to type *C* β-scission, which involves a secondary 2-methylpentyl-4 carbenium ion [41]. The presence of butanes and pentanes suggests that these hydrocarbons originate from the cracking of C_{12} reaction intermediates, when the reaction is governed by the dimerisation-cracking mechanism. Transformation of *n*-hexane via the dimerisation-cracking mechanism is confirmed by the ζ values, which in many instances are lower than 2.

As shown by the data in Table 6, the $C_4 + C_5$ cracking products are characterised by low *i/n* ratios (also observed by Lugstein et al. [42] over Ni/ZSM-5). In the 10-membered ring channel, bulky α, γ, γ-tribranched alkylcarbenium ions (whose formation is assumed to be governed by the dimerisation-cracking mechanism) cannot form because of steric hindrance, and that is why type *A* and type

Table 5 Conversion of *n*-hexane and the yield of the reaction products at selected reaction temperatures

Code	T (°C)	C_1–C_5 yield (wt%)	i-C_6 yield (wt%)	HBH yield (wt%)	Conversion (%)
A/F + I	250	0.2	6.7	0.0	6.9
	300	20.0	12.4	0.0	32.4
	350	55.1	4.4	13.9	73.4
	400	35.2	0.0	60.8	96.0
A/F	250	2.1	7.5	3.1	12.7
	300	24.0	6.7	9.2	39.9
	350	37.5	2.2	36.4	76.1
	400	14.0	1.5	73.0	88.5
E/I	250	9.5	4.0	1.7	15.2
	300	25.6	4.5	9.2	39.3
	350	16.1	2.5	56.0	74.6
	400	19.7	1.1	74.1	94.9
E/F + I	250	2.4	12.0	0.3	14.7
	300	25.5	15.3	1.0	41.8
	350	55.8	3.0	14.0	72.8
	400	22.9	0.8	72.5	96.2
E/F	250	1.5	4.0	0.0	5.5
	300	27.1	5.9	0.3	33.3
	350	44.9	2.0	27.1	74.0
	400	22.7	0.4	73.3	96.4

B_1 β-scissions do not occur; products are generated via β-scission of two- or mono-branched alkylcarbenium ions (β-scissions of type B_2 and type C) [41]. This is the reason why the *i*/*n* ratios of the cracking products are low in constrained environments. According to Soualah et al. [43], *i*/*n* ratios lower than 1 suggest that the cracking products originated from mono-branched isomers.

With all the catalysts examined, the main isomerisation products are monobranched pentanes, and 2-methylpentane is favoured against 3-methylpentane (Table 6). Such distribution in the presence of Pt/H-ZSM-5 has been observed by Yashima et al. [44]. They have furthermore found that the amounts of 2-methylpentane are higher in the medium-pore zeolite ZSM-5 than in large-pore zeolites (mordenite, BETA). Preferential formation of 2-methyl- over 3-methylbranched hydrocarbons is a manifestation of transition state shape selectivity [41]. The channels of ZSM-5 are insufficiently large to enable the production of two-branched isomers. They undergo cracking to a large extent because it is difficult for them to leave the pores of the zeolite channels.

Selectivity to isomerisation products (*i*-C_6) is higher over E/F + I and A/F + I than over E/F and A/F catalysts (Fig. 10c). This can be attributed to the weaker interactions between Ni and support in catalysts prepared by the method of two-stage nickel incorporation. The ratio of the number of accessible nickel atoms (n_{Ni_a}) to the number of acid sites (n) for E/F + I and A/F + I is 3.2×10^{-2} and 4.8×10^{-2}, respectively, whereas that for A/F and E/F amounts to 1.2×10^{-2} and 1.8×10^{-2}, respectively (Table 3). Despite the seemingly slight differences between these ratios, the number of metal sites in the catalysts with higher ratios is large enough for the isomerised carbenium ions to undergo hydrogenation and leave the catalyst surface prior to cracking.

Table 6 Distribution of isomerisation (S_{HI}), cracking (S_{HK}) and HBH (S_{HBH}) products

Code	Conversion (%)	h/c ratio	Fragmentation factor, ζ	i/n ratio for $C_4 + C_5$
A/F + I	15–73	0.2–0.3	1.9–2.2	0.5–0.7
A/F	13–76	0.1–0.2	1.7–2.0	0.5–0.7
E/I	15–75	<0.1–0.2	1.5–1.9	0.7–0.9
E/F + I	15–73	0.1–0.4	1.4–2.3	0.6–0.9
E/F	17–74	~0.1	1.5–1.9	0.6–0.7

Although Ni–alumina interactions in catalyst E/I are relatively weak (Ni^0/Ni_{total}, 18 at%; n_{Ni_a}/n, 2.7×10^{-2}), selectivity to *i*-C_6 is very low. This can probably be attributed to the noticeably long distance from metal sites (mainly on the external grain surface) to acid sites (mainly inside the zeolite channel) as well as to the blocking of zeolite channels by metal clusters (low V_{MIC}, Table 1). The separated metal sites catalyse the dehydrogenation of *n*-C_6 followed by cyclisation, which produces HBH (Fig. 10d).

The slightly higher HBH yield up to 300 °C over A/F may be associated with the lower reducibility of this catalyst caused by the strong metal-support interaction. As a result of decreased reducibility, the proportion of Ni^{2+} on the surface of catalyst A/F is higher as compared with the other catalysts (Table 3). According to Hoang et al. [45] the occurrence of the synergic effect between Ni^{2+} acting as Lewis sites and Brønsted acid sites increases catalyst activity in the aromatisation of *n*-C_6.

4 Conclusions

1. Regardless of the method used for combining zeolite and alumina or nickel incorporation, metal-support interactions in NiO(8 %)/ZSM-5 + Al_2O_3(1:1) catalysts are strong. When the nickel precursor was incorporated before catalyst shaping, metal-support interactions were only slightly stronger (D = 0.9–1.5 %, 7–9 at% Ni^0, the ratio of the accessible number of metal sites to the number of acid sites (n_{Ni_a}/n), 1.2×10^{-2} and 1.8×10^{-2}) than when the nickel precursor was deposited by single-stage impregnation of the shaped support or by the two-stage method using

impregnation at the second stage ($D = 2.2$–3.7 %, 11–18 at.% Ni^0, n_{Ni_a}/n, 2.7×10^{-2}–4.8×10^{-2}).

2. Over the catalysts with weaker Ni–alumina interactions (n_{Ni_a}/n, 3.2×10^{-2} and 4.8×10^{-2}), selectivity to isomerisation products was by 10–35 % higher, and selectivity to high boiling hydrocarbons by 10–30 % lower compared to the catalysts with stronger Ni-support interactions (n_{Ni_a}/n, 1.2×10^{-2} and 1.8×10^{-2}).
3. Although the E/I catalyst (nickel precursor was deposited by single-stage impregnation of the shaped support) is characterised by a relatively high metal-to-support ratio (n_{Ni_a}/n, 2.7×10^{-2}), the yield of isomerisation products was low, while the yield of HBH products was high, which should be attributed to the dehydrogenation and cyclisation of n-C_6 that occur over the "isolated" metal sites.
4. Because of steric hindrance, Ni–alumina interactions do not influence the composition of isomerisation and cracking products:
   - the main isomerisation products are monobranched hexanes, and the 2-methylpentane is favoured against the 3-methylpentane
   - $C_4 + C_5$ cracking products (obtained mainly via the dimerisation-cracking mechanism) are characterised by a low extent of isomerisation, which suggests that they were generated by B_2 or C type β-scission of C_{12} alkylcarbenium ions.

Acknowledgments Studies on catalyst activity were supported by the Polish Ministry of Science and Higher Education (S20065/Z0306).

References

1. Gronchi P, Kaddouri A, Centola P, Rosso RD (2003) J Sol Gel Sci Technol 26:843–846
2. Romero M, Lukas DA, Calles JA, Rodriguez A (1996) Appl Catal A 46:425–441
3. Galperin LB, Bradley SA, Mezza TM (2001) Appl Catal A 219:79–88
4. Canizares P, De Lucas A, Dorado F, Duran A, Ascencio I (1998) Appl Catal A 169:137–150
5. Perego C, Villa P (1997) Catal Today 34:281–305
6. Gavrilidis A, Varma A (1993) Catal Rev Sci Eng 35:399–456
7. Akhmedov VM, Al-Khowaiter SH, Al-Refai JK (2003) Appl Catal A 252:353–361
8. Lekhal A, Glasser BJ, Khinast JG (2004) Chem Eng Sci 59:1063–1077
9. Pinna F (1998) Catal Today 41:129–137
10. Reymond JP, Kolenda F (1999) Powder Technol 103:30–36
11. Schreier M, Regalbuto JR (2004) J Catal 225:190–202
12. Geus JW, van Veen JAR (1993) Stud Surf Sci Catal 79:335–362
13. Liu BS, Au CT (2003) Appl Catal A 244:181–195
14. Znak L, Zielinski J (2008) Appl Catal A 334:268–276
15. Minchev C, Zubkov SA, Valtchev V, Minkov V, Micheva N, Kanazirev V (1994) Appl Catal A 119:195–204
16. Richardson JT, Twigg MV (1998) Appl Catal A 167:57–64
17. Twigg MV, Richardson JT (2000) Appl Catal A 190:61–72
18. Szegedi Á, Popova M (2010) J Porous Mater 17:663–668
19. Liu Y, Chen J, Zhang J (2007) Chin J Chem Eng 15:63–67
20. Monteiro-Gezork AC, Effendi A, Winterbottom JM (2007) Catal Today 128:63–73
21. Salagre P, Fierro JLG, Medina F, Sueiras JE (1996) J Mol Catal A 106:125–134
22. Barrio VL, Arias PL, Cambra JF, Güemez MB, Campos-Martin JM, Pawelec B, Fierro JGL (2003) Appl Catal A 248:211–225
23. Barrio VL, Arias PL, Cambra JF, Güemez MB, Pawelec B, Fierro JLG (2004) Catal Commun 5:173–178
24. Lif J, Odenbrand I, Skoglundh M (2007) Appl Catal A 317:62–69
25. Wang R, Li Y, Shi R, Yang M (2011) J Mol Catal A 344:122–127
26. Sepúlveda J, Fígoli NS (1995) React Kinet Catal Lett 55:383–389
27. Blomsma E, Martens JA, Jacobs PA (1996) J Catal 159:323–331
28. Abbot J, Wojciechowski BW (1985) Can J Chem Eng 63: 451–461
29. Jiménez C, Romero FJ, Roldán R, Marinas JM, Gómez JP (2003) Appl Catal A 249:175–185
30. Guisnet M, Magnoux P (2001) Appl Catal A 212:83–96
31. Huybrechts W, Thybaut JW, De Waele BR, Vanbutsele G, Houthoofd KJ, Bertinchamps F, Denayer JFM, Gaigneaux EM, Marin GB, Baron GV, Jacobs PA, Martens JA (2006) J Catal 239:451–459
32. Masalska A (2005) Appl Catal A 294:260–272
33. Long-Xiang T, Feng-Mei Z, Lu-Bin Z (1996) React Kinet Catal Lett 57:99–104
34. Pawelec B, Mariscal R, Navarro RM, Campos-Martin JM, Ferro JLG (2004) Appl Catal A 262:155–166
35. Rynkowski JM, Paryjczak T, Lennik M (1993) Appl Catal A 106:73–82
36. Heracleous E, Lee AF, Wilson K, Lemonidou AA (2005) J Catal 231:59–171
37. Li CH, Chen YW (1995) Thermochim Acta 256:457–465
38. Li G, Hu L, Hill JM (2006) Appl Catal A 301:16–24
39. Petti TF, Tomczak D, Pereira CJ, Cheng WC (1998) Appl Catal A 169:95–109
40. Kharat AN, Pendleton P, Badalyan A, Abedini M, Amini MM (2002) J Catal 205:7–15
41. Jacobs PA, Martens JA (1991) Stud Surf Sci Catal 58:445–451
42. Lugstein A, Jentys A, Vinek H (1999) Appl Catal A 176:119–128
43. Soualah A, Lemberton JL, Pinard L, Chater M, Magnoux P, Moljord K (2008) Appl Catal A 336:23–28
44. Yashima T, Wang ZB, Kamo A, Yoneda T, Komatsu T (1996) Catal Today 29:279–283
45. Hoang DL, Berndt H, Miessner H, Schreier E, Völter J, Lieske H (1994) Appl Catal A 114:295–311